

# Inflammation plays a critical role in damage to the bronchiolar epithelium induced by *Trueperella pyogenes* in *vitro* and *in vivo*

Lei Qin<sup>1,4#</sup>, Fandan Meng<sup>1#</sup>, Haijuan He<sup>5</sup>, Siqi Li<sup>1</sup>, Hongliang Zhang<sup>1</sup>, Yuan Sun<sup>1</sup>,  
Wenlong Zhang<sup>4</sup>, Tongqing An<sup>1</sup>, Xuehui Cai<sup>1,3\*</sup>, Shujie Wang<sup>1,2\*</sup>

<sup>1</sup> State Key Laboratory for Animal Disease Control and Prevention, Harbin Veterinary  
Research Institute, Chinese Academy of Agricultural Sciences, Harbin 150001,  
Heilongjiang, PR China; <sup>2</sup> Heilongjiang Provincial Key Laboratory of Veterinary  
Immunology, Harbin, China; <sup>3</sup> Heilongjiang Research Center for Veterinary  
Biopharmaceutical Technology; <sup>4</sup> College of Veterinary Medicine, Northeast  
Agricultural University, Harbin 150030, Heilongjiang, PR China; <sup>5</sup> Institute of  
Animal Husbandry, Heilongjiang Academy of Agriculture Sciences, Harbin 150086,  
Heilongjiang, PR China.

**Running title:** *Trueperella pyogenes* damages bronchiolar epithelium

# These authors contributed equally

**\*Correspondence:** State Key Laboratory of Veterinary Biotechnology, Harbin  
Veterinary Research Institute of Chinese Academy of Agriculture Science, Harbin,  
150069, China. Tel: +86 451-51051766; E-mail: caixuehui@caas.cn;  
wangshujie@caas.cn

## 23 Abstract

24 *Trueperella pyogenes* can cause severe pulmonary disease in swine, but the  
 25 mechanism of pathogenesis is not well defined. *T. pyogenes*-induced damage to  
 26 porcine bronchial epithelial cells (PBECs), porcine precision-cut lung slices (PCLS)  
 27 and respiratory epithelium of mice remains unknown. In this study, we used *T.*  
 28 *pyogenes* 20121 to infect PBECs in air-liquid interface conditions and porcine PCLS.  
 29 *T. pyogenes* could adhere to, colonize and induce cytotoxic effect on PBECs and the  
 30 luminal surface of bronchi in PCLS, which damaged the bronchiolar epithelium.  
 31 Moreover, bronchiolar epithelial cells showed extensive degeneration in infected mice  
 32 lungs. Furthermore, western blot showed the NOD-like receptor (NLR)/ C-terminal  
 33 caspase recruitment domain (ASC)/caspase-1 axis and nuclear factor-kappa B (NF- $\kappa$ B)  
 34 pathway were involved in inflammation in PCLS and lungs of mice, which also  
 35 confirms PCLS provide a platform to analyze pulmonary immune response.  
 36 Meanwhile, the levels of p-c-Jun N-terminal kinase (JNK), p-extracellular  
 37 signal-regulated kinase (ERK) and p-protein kinase B (AKT) were increased  
 38 significantly, which indicated the mitogen-activated protein kinase (MAPK) and Akt  
 39 pathways were also involved of inflammation in *T. pyogenes*-infected mice. In  
 40 addition, we used *T. pyogenes* 20121 to infect tumour necrosis factor alpha (TNF- $\alpha$ )<sup>-/-</sup>  
 41 mice, the results indicated apoptosis and injury in respiratory epithelium of infected  
 42 TNF- $\alpha$ <sup>-/-</sup> mice were alleviated. Thus, pro-inflammatory cytokine TNF- $\alpha$  played a role  
 43 in apoptosis and respiratory epithelium injury of mice lungs. Collectively, our study  
 44 provides an insight into the inflammatory injury induced by *T. pyogenes*, and suggests

45 that blocking NLR or TNF- $\alpha$  may be a potential therapeutic strategy against *T.*

46 *pyogenes* infection.

47 **Key words:** *Trueperella pyogenes*, PBECs, PCLS, Infection, Inflammation, Pathways

48

## 49     **Introduction**

50     *T. pyogenes* is frequently isolated from pyogenic disease conditions in both domestic  
51     and wild animals worldwide, but is rare in companion animals and humans. *T.*  
52     *pyogenes* also plays an important role in secondary infection and co-infection in  
53     domestic animals (1, 2). In swine, *T. pyogenes* is a common opportunistic pathogen  
54     found in pneumonia, endocarditis, pleuritis and organ abscesses (3, 4), and it is an  
55     emerging clinical, epidemiological and economic problem on pig farms (5). Although  
56     pneumonia in swine with airway inflammation caused by *T. pyogenes* is a frequent  
57     occurrence (6), the mechanisms of pathogenesis remain poorly understood.

58     The primary route of infection for many respiratory pathogens is the airway, which is  
59     lined by a layer of epithelial cells that form a primary barrier (7). Thus,  
60     well-differentiated porcine bronchial epithelial cells (PBECs) in air-liquid interface  
61     (ALI) conditions, which provide a close *in vitro* model of the airway epithelium (8, 9),  
62     have been used to study bacterial infections (10, 11). Precision-cut lung slices (PCLS)  
63     as ex-vivo lung culture can mimic the immediate and long-term functional responses  
64     of the respiratory tract and lung (12-14), which allows studies on inflammatory  
65     responses induced by respiratory pathogens (15, 16). Moreover, the 3D respiratory  
66     organotypic tissue reflects the natural microanatomy and microenvironment of the  
67     respiratory system (14), permitting a reduction in the number of laboratory animals  
68     used (33, 29).

69     Little is known about inflammatory response and mechanism of bronchial damage of  
70     *T. pyogenes* infections *in vitro* or *in vivo*, though we recently used PCLS to study the  
71     pathogenicity of a novel isolate (17). In the present study, ALI cultures, PCLS and



mice were used to analyze the adherence and colonization of *T. pyogenes* to porcine airway epithelial cells, seeking to further elucidate how the bacterium damages the respiratory tract.

## **Materials and Methods**

### **Bacterial strain and growth conditions**

The virulent strain *T. pyogenes* 20121 was isolated from the lungs of sick pigs from a pig farm as previously described (17) and stored in our lab. *T. pyogenes* 20121 was grown in tryptic soy broth (TSB; Difco, Loveton Circle Sparks, MD, USA) supplemented with 5% fetal bovine serum (FBS; CLARK, USA) or on Columbia-based blood agar media (ThermoFisher Scientific, China) at 37 °C. For preparation of cryo-conserved bacterial stocks, *T. pyogenes* was grown in TSB medium until late exponential growth phase ( $OD_{600nm} = 0.5$ ). Bacteria were harvested by centrifugation (3000 g for 5 min at 4 °C), washed once with phosphate-buffered saline (PBS) and re-suspended in TSB medium containing 50% (v/v) glycerol. Aliquots were immediately shock frozen in liquid nitrogen and stored at -80 °C until use.

### **Infection of well-differentiated PBECs by *T. pyogenes***

Porcine lungs were obtained from specific pathogen free (SPF) pigs, and primary PBECs were harvested from the bronchi as previously described (11). Briefly, PBECs were scraped carefully from the luminal surface of the bronchus without disturbing the mucosal surface integrity and cultured in bronchial epithelial cell growth medium (BEBM; Lonza, Belgium) supplemented with antibiotics. When PBECs reached about 80% confluence, they were seeded on 0.4 µm pore size transwell filters with

95 polycarbonate membranes (Corning Costar, USA). Cells were then cultured at 37 °C  
96 with 5% CO<sub>2</sub> with ALI medium as described previously (18), which is mixture of  
97 BEBM and DMEM at 1:1 supplemented with antibiotics. At 3 days post-seeding,  
98 cultures were maintained under ALI conditions for an additional 4 weeks at 37 °C  
99 with 5% CO<sub>2</sub> for epithelial cell differentiation, changing the culture medium every  
100 two days.

101 Growth characteristics of *T. pyogenes* 20121 was determined on PBECs that cultured  
102 under air-liquid interface condition for 4 weeks, and all treatments were repeated at  
103 least three times. Transwell filters were washed 3 times with PBS and cultured in  
104 fresh medium without antibiotics for 24 h prior to infection. *T. pyogenes* 20121 was  
105 inoculated into the apical compartment with approximately 8×10<sup>5</sup> CFU per filter, and  
106 the supernatant from apical compartment was collected for a cytotoxicity assay after 4  
107 h at 37 °C with 5% CO<sub>2</sub>. Both apical and basolateral compartments were washed 3  
108 times with PBS to remove any non-adherent bacteria, and maintained under ALI  
109 condition. Cytotoxicity assays and immunofluorescence on PBECs were performed at  
110 4 h post-inoculation (hpi), 24 hpi, 48 hpi and 72 hpi.

# 111 **Infection of *T. pyogenes* on porcine PCLS**

112 The cranial, middle and intermediate lobes were harvested from fresh lung tissue of  
113 three sacrificed SPF pigs. Each lobe was gently filled with 1.5% (w/v) warming  
114 low-melting agarose (Promega, USA) along the bronchus as described previously (19).  
115 The lobes were stamped out with an 8-mm tissue coring tool, and after the agar was  
116 solidified, slices were prepared on a Krumdieck tissue slicer (model MD6000-01;

117 TSE Systems, USA) with 6-10 slices per minute. Next, the PCLS were carefully  
 118 transferred into 24-well plates and maintained with 1 mL fresh RPMI medium 1640  
 119 supplemented with antibiotics (including 80 µg/ml kanamycin, 10 µg/ml enrofloxacin,  
 120 5 µg/ml levofloxacin, 2.5 µg/ml amphotericin, 50 µg/ml ciprofloxacin), and the  
 121 medium was refreshed per hour to remove the agarose and repeat for 3 times, then  
 122 cultured overnight. PCLS containing bronchia and showing 100% ciliary activity  
 123 were selected by light microscopy (EVOS FL Auto; Thermo Fisher Scientific, USA)  
 124 for subsequent experiments. RPMI medium 1640 without antibiotic or antimycotic  
 125 was added 24 h prior to bacterial infection studies. PCLS were washed 3 times with  
 126 PBS, then inoculated with *T. pyogenes* at  $8 \times 10^4$  (3 slices) or  $8 \times 10^5$  CFU (3 slices) per  
 127 slice at 37 °C, and the control group (mock-infected slices, 6 slices total) was cultured  
 128 normally under the same conditions. The experiment was repeated three times (a pig  
 129 per time, 3 pigs total). At 4 hpi, slices were washed three times with PBS to remove  
 130 non-attached bacteria, and 1 mL fresh RPMI medium 1640 (Gibco, Beijing, China)  
 131 was added for further cultivation. The areas of bronchial cavity were measured and  
 132 calculated by ImageJ/Fiji software, and bronchial contraction percentage (BCP)  
 133 presented the results using the following formula,  $BCP = [\text{reduced bronchial cavity}$   
 134  $\text{area} / \text{initial bronchial cavity area}] \times 100\%$ . The supernatant was collected at 4 hpi, 24  
 135 hpi and 72 hpi for cytotoxicity assays, and PCLS were homogenized in PBS and then  
 136 serially diluted and plated onto TSA for enumeration of bacteria.

### 137 **Cytotoxicity assay**

138 The release of lactate dehydrogenase (LDH, Promega, USA) into the culture medium

139 was quantitated using Cyto Tox 96® Non-Radioactive Cytotoxicity Assay (Promega,  
140 Madison, WI, USA) as described previously (20). To determine the cytotoxic effect  
141 caused by *T. pyogenes* 20121, 50 µL of supernatant from infected or mock-infected  
142 PBECs or PCLS at each time point was mixed with an equal volume of substrate mix  
143 reagent in the dark. The detected supernatant in PBECs were obtained by washing the  
144 upper chamber of transwell for 20 minutes using culture medium on the shaker at 24,  
145 48, 72 hpi. After 30 min, stop solution was added and absorbance signal was  
146 measured at 490 nm. The results were compared with the control group and presented  
147 as 100% cytotoxicity. Three parallel PBECs or PCLS (from the same pig) in different  
148 infected groups were collected at each detection time, and the infected experiments  
149 were repeated three time (a pig per time, 3 pigs total). The cytotoxicity assay in  
150 PBECs or PCLS were replicated three times.

# 151 **Animal experiments**

152 All animal experiments were performed in accordance with the Guide for the Care  
153 and Use of Laboratory Animals of the Ministry of Science and Technology of the  
154 People's Republic of China. Mouse infection experiments (approval number  
155 210119-02) were carried out in the animal biosafety level 2 facilities under  
156 supervision of the Committee on the Ethics of Animal Experiments of the Harbin  
157 Veterinary Research Institute of the Chinese Academy of Agricultural Sciences  
158 (CAAS) and the Animal Ethics Committee of Heilongjiang Province, China.  
159 7-week-old female C57BL/6 wild type (WT) mice (Changsheng Biotechnology,  
160 Liaoning, China) were randomly divided into 2 groups. Uninfected controls (n=12)

received 0.2 mL TSB intraperitoneally (i.p.), and the rest (n=20) were challenged i.p. with 0.2 mL TSB containing  $2 \times 10^6$  CFU *T. pyogenes* 20121. Lung and blood samples from infected mice (n=5) and control (n=3) were aseptically harvested after 1, 2, 4 and 7 days post-infection (dpi) for histopathological analysis and cytokine detection. Bacterial load in lungs and blood were monitored as previously described (21), briefly, anticoagulated blood and lung samples were serially diluted, and plated on blood agar medium for 36 h, and the bacteria were quantified by colony counting. In a separate experiment, 16 female TNF- $\alpha^{-/-}$  C57BL/6N mice were purchased from Cyagen Biosciences (Santa Clara, USA), and at 6-7 weeks-of-age were randomly divided into 2 groups. Uninfected controls (n=6) received 0.2 mL TSB i.p., and the other group was inoculated i.p. with *T. pyogenes* 20121 as above. 5 infected TNF- $\alpha^{-/-}$  mice and 3 uninfected TNF- $\alpha^{-/-}$  mice were humanely euthanized at 1 and 2 dpi, Lung and blood samples were harvested, and lung tissue samples were fixed in 3.7% formaldehyde (Amresco, Fountain Parkway, USA) for further histopathological analysis. Lung samples were sectioned (8- $\mu$ m-thick slices) on a cryostat and used for double-immunofluorescence staining.

# **Cryosections and immunofluorescence analysis**

PCLS were washed 3 times using PBS to remove unattached bacteria, embedded on filter paper by tissue freezing medium (Sigma-Aldrich, USA) and quickly frozen in liquid nitrogen, then stored at -80 °C. 10- $\mu$ m-thick cryo-slices were produced by a cryostat (Thermo, USA) and stored at -20 °C. The slices were dried at room temperature (RT) prior to immunofluorescence analysis.

183 PBECs and cryosection samples were fixed with 3.7% paraformaldehyde (Amresco,  
184 Fountain Parkway, USA) for 30 min, followed by 0.1 M glycine treatment for 20 min  
185 at RT. After three washing steps with PBS, samples were permeabilized with 0.2%  
186 Triton X-100 (Sigma-Aldrich, USA) for 20 min at RT. 1% (v/v) bovine serum  
187 albumin (BSA; biofroxx, Germany) was used to block nonspecific reactions for 30  
188 min at RT. The primary antibody for detection of *T. pyogenes* was polyclonal mouse  
189 antiserum (1: 300, made in our lab), and ciliated cells were stained using a  
190 Cy3-labeled anti- $\beta$ -tubulin monoclonal antibody (1:300; Sigma-Aldrich, USA). Alexa  
191 Fluor<sup>®</sup> 488-labeled goat-anti-mouse IgG (H+L) (1:1000; Thermo Fisher Scientific,  
192 USA) was used as secondary antibody; all antibodies were diluted in 1% BSA. Nuclei  
193 were stained with DAPI (4',6-diamidino-2-phenylindole; Cell Signaling Technology,  
194 USA), and finally samples were mounted with ProLong<sup>®</sup> Gold Antifade Reagent  
195 (Thermo Fisher Scientific, USA) and stored at 4 °C with light protection. Slides were  
196 examined on a confocal laser scanning microscopy with fast Airyscan  
197 (LSM980-ZEISS, Germany), and Z-stack images were acquired containing 0.22  $\mu$ m  
198 per plane. Maximum intensity projections were calculated for display purposes and  
199 adjusted for brightness and contrast using ZEN 2.3 blue software.

200 Lung samples collected at necropsy were sectioned (7  $\mu$ m-thick) and used for  
201 apoptosis detection. To confirm the cells of lungs that underwent apoptosis, lung  
202 sections were stained with rabbit anti-mouse caspase-3 antibody (1:500, Cell  
203 Signaling, MA, USA) and Alexa Fluor<sup>™</sup> 488-conjugated goat anti-rabbit antibody  
204 (1:1000, Sigma, Missouri, USA); Apoptosis also was detected using a terminal

205 deoxynucleotidyl transferase (TdT)-mediated deoxyuridine triphosphate  
206 (dUTP)-biotin nick end-labeling (TUNEL) assay with Cell Death Detection Kit  
207 (Roche, Germany). Nuclei were stained with 4-6-diamidino-2-phenylindole (DAPI,  
208 Sigma).

## 209 **Western blot analysis**

210 Lung samples from the PCLS and mice were lysed in RIPA buffer containing the  
211 protease inhibitors PMSF (Solarbio, China) and Complete Protease Inhibitor  
212 (EDTA-free; Merck-Millipore, Germany). Protein concentration was quantified using  
213 a BCA Protein Assay Kit (Beyotime Institute of Biotechnology, China). Equal  
214 amounts of protein were loaded and separated by electrophoresis on 12% SDS-PAGE  
215 gels and subsequently transferred to polyvinylidene fluoride (PVDF; Merck-Millipore,  
216 Germany). After blocking with 10% skim milk for 1 h, the membranes were incubated  
217 at room temperature for 1 h with the antibodies about the inflammasome, including  
218 the rabbit anti-NLRP1, NLRC4, gasdermin D (GSDMD), GSDMD-C (1:1,000,  
219 abcam), IL-1 $\beta$ , IL-4, IL-18, matrix metalloproteinase 9 (MMP9), macrophage  
220 migration inhibitory factor (MIF) (1:500, ABclonal), NLRP3, caspase-1 p20 and the  
221 mouse anti-ASC (1:1,000, these three antibodies were kindly provided by Professor  
222 Changjiang Weng of Harbin Veterinary Research Institute of Chinese Academy of  
223 Agricultural Sciences (22). The rabbit anti-AKT1/2/3 and phospho-AKT1/2/3, p38  
224 and phospho-p38, ERK1/2 and phospho-ERK1/2, JNK1/2/3 and phospho-JNK1/2/3,  
225 NF- $\kappa$ B p65 and phospho-NF- $\kappa$ B p65 (1:1,000, abcam) were prepared for the tests of  
226 MAPK, Akt and NF- $\kappa$ B signaling pathways. Furthermore, antibodies related to

apoptosis, including the rabbit anti-Caspase-8, Caspase-9, Caspase-3 and apoptosis inducing factor (AIF) (1:1,000, abcam) were also used in this process. Expression of all the target proteins were normalized to that of the internal control rabbit/mouse antibodies against  $\beta$ -actin or GADPH (1:50,000, ABclonal). Relevant DyLight™ 800-labeled goat anti-rabbit/-mouse IgG (H+L) secondary antibodies were applied as needed (SeraCare, KPL Antibodies & Conjugates, USA). The relative integrated density of the target protein to the internal control was quantified using Image J v1.8.0 software (Wayne Rasband, National institutes of Health, USA) and then the relative quantitative comparison was shown after the normalization of the relative integrated density of the control group.

### **Detection of cytokine production in PCLS or mice**

To quantify the cytokines induced by *T. pyogenes* infection, supernatants from infected PCLS were collected at 4 hpi, 24 hpi and 72 hpi, and the quantity of interleukin (IL)-4, IL-10 and chemokine CXCL8 was determined by ELISA according to the manufacturer's instructions (USCN Life Sciences, China). The quantity of IL-1 $\beta$ , IL-6, IL-10, TNF- $\alpha$  and IFN- $\gamma$  was also determined in serum samples collected from infected mice at 1, 2, 4 and 7 dpi by commercial ELISA according to the manufacturer's instructions (Cusabio, China).

### **Statistical analyses**

All experiments were performed at least three times, and results are expressed as the mean  $\pm$  standard deviation (SD). Statistical analysis of the results was performed with one- or two-way analysis of variance (ANOVA) using GraphPad Prism software



249 version 9.00 (GraphPad, San Diego, CA, USA). A *P* value < .05 was considered

250 statistically significant.

251

## 252     **Results**

### 253     ***T. pyogenes* infection induces epithelium damage on well-differentiated PBECs**

254     The infection of well-differentiated PBECs by *T. pyogenes* was first analyzed under  
 255     ALI conditions. *T. pyogenes* induced cytotoxic effects as early as 4 h post-infection in  
 256     comparison to mock-infected PBECs (Fig. 1A). No significant cytotoxic effect was  
 257     detected at 24 hpi in comparison to mock-infected PBECs, but cytotoxic effect was  
 258     significantly enhanced at 48 hpi. Attachment of *T. pyogenes* to epithelial cells under  
 259     ALI condition was detected by confocal microscopy (Fig. 1B). Tiny microcolonies of  
 260     *T. pyogenes* were observed adhering to the cilia of ciliated cell at 4 hpi. The size of the  
 261     microcolonies increased by 24 hpi, indicating *T. pyogenes* was able to proliferate on  
 262     the epithelial cells under ALI condition. Notably, *T. pyogenes* caused severe damage  
 263     to the epithelial cells and the cilia after infection, and epithelial integrity was lost by  
 264     72 hpi. Importantly, *T. pyogenes* crossed the epithelial cell layer and reached the  
 265     membrane of the transwell filter.

### 266     **Adhesion and colonization of *T. pyogenes* on the luminal surface of bronchi in** 267     **porcine PCLS**

268     To investigate the adhesion and colonization characteristics, porcine PCLS were  
 269     infected or mock-infected by *T. pyogenes* 20121. Bronchoconstriction was induced by  
 270     bacterial infection in a dose-dependent manner (Fig. 2A). At  $8 \times 10^5$  CFU/slice, *T.*  
 271     *pyogenes* caused notable bronchoconstriction (BCP: 94.46%, 87.18%, 84.91%,  
 272     respectively), while slighter constriction (BCP: 62.69%, 70.09%, 75.02%,  
 273     respectively) was seen with  $8 \times 10^4$  CFU/slice at 4, 24 and 72 hpi. *T. pyogenes* adhered

in microcolonies to the luminal surface of bronchi that was presented by the ciliated epithelial cell layer (Fig. 2A). Proliferation of *T. pyogenes* was not affected by bronchoconstriction, with colonizing bacteria still able to proliferate in the constricted area of bronchioles, as indicated by the arrow (Fig. 2A, 24 hpi). Infection with  $8 \times 10^5$  CFU of *T. pyogenes* also caused more severe injury to the ciliated epithelial layer than the lower dose at 72 hpi (Fig. 2A). Meanwhile, the CFU counts in the PCLS slice lysate also showed much higher numbers at 24 and 72 hpi than at 4 hpi (Fig. 2B), confirming the proliferation of *T. pyogenes*. Additionally, the  $8 \times 10^5$  CFU-infected group had more bacteria attached ( $>10^5$  CFU) than the  $8 \times 10^4$  CFU infected group ( $10^4$  CFU) at 24 hpi, whereas no significant difference was detected at 72 hpi.

As a measure of cytotoxicity, the amount of LDH released from infected PCLS was determined. *T. pyogenes* induced significant cytotoxic effect on PCLS at 4 and 24 hpi, and the high-dose group caused greater cytotoxicity than the low-dose group (Fig. 2C). The low-dose infection group caused slightly higher cytotoxicity than the high-dose group at 72 hpi, which may be related to a decrease in the number of ciliated epithelial cells due to the more serious damage caused by the high-dose infection.

## 290 **Secretion of inflammatory cytokines into the supernatant of infected porcine**

### 291 **PCLS**

To understand the immune response triggered by *T. pyogenes* in PCLS, the amount of cytokines released into supernatant were measured. Anti-inflammatory cytokines IL-4 and IL-10 in supernatant (Fig. 2D and E) were secreted at 4 hpi, which was earlier than secretion of the chemokine CXCL8 (Fig. 2F). The level of IL-4 in supernatant of

both infected groups was significantly higher ( $P < .001$ ) than mock infection at 4 and 24 hpi, and IL-10 increased significantly by 4 hpi only in the high-dose group. Western blot analysis also confirmed an upregulation of IL-4 in PCLS tissue infected with  $8 \times 10^5$  CFU at 4, 24 and 72 hpi (Fig. 2G). However, chemokine CXCL8 was notably upregulated in supernatant of *T. pyogenes*-infected PCLS by 24 and 72 hpi compared with mock infection.

### ***T. pyogenes* activated the NLRP3 and NF- $\kappa$ B pathways in porcine PCLS**

To investigate the effect of the NLRP3 inflammasome on the *T. pyogenes*-induced inflammatory response, PCLS were collected for western blot analysis. *T. pyogenes* infection activated NLRP3 inflammasome, with NLRP3 expression enhanced significantly from 4 hpi to 72 hpi (Fig. 3A), and ASC expression was also enhanced from 4 hpi to 72 hpi compared to control, although it also suggests a drop from 4 h to 24h (Fig. 3B). Meanwhile, pro-caspase-1 was activated and cleaved, with caspase-1 (p20) enhanced significantly at 24 and 72 hpi (Fig. 3C). Furthermore, inflammatory cytokines IL-1 $\beta$  and IL-18 expression were upregulated from 4 to 72 hpi compared to control, but a slight drop in 72 hpi compared to 24 hpi (Fig. 3D and E). In addition, NF- $\kappa$ B and two important factors (MMP9 and MIF) that participate in inflammation were analyzed. Expression of MMP9 increased significantly from 4 to 72 hpi (Fig. 3F) and expression of MIF increased strikingly at 24 and 72 hpi (Fig. 3G) compared to control. Expression of NF- $\kappa$ B increased substantially at 24 hpi and 72 hpi compared to control. These results suggest that the NLRP3 inflammasome and NF- $\kappa$ B pathways are both activated in PCLS infected with *T. pyogenes*.

### 318 ***T. pyogenes* damages the respiratory tract of infected mice**

319 To examine the effect of *T. pyogenes* infection on the development of associated  
320 pulmonary pathology in a live animal model, six-week-old C57BL/6 mice were i.p.  
321 inoculated with *T. pyogenes* or TSB, and the histopathological changes in the lungs or  
322 tracheas were examined at 1, 2, 4 and 7 dpi. The lungs of *T. pyogenes*-infected mice  
323 exhibited mild degeneration of bronchiolar epithelial cells with marked infiltration of  
324 inflammatory cells in the bronchial epithelium at 1 and 2 dpi (Fig. 4A). Furthermore,  
325 the bronchiolar epithelial cells were extensively degenerated at 4 dpi, and the  
326 adventitia showed mild edema in addition to degeneration of bronchiolar epithelial  
327 cells at 7 dpi. Compared with mock-infected mice, massive degeneration of tracheal  
328 epithelial cells was observed in mice infected with *T. pyogenes* from 1 to 4 dpi, and  
329 nuclear concentration of tracheal epithelial cells was observed at 7 dpi (Fig. 4B). Thus,  
330 *T. pyogenes* infection caused significant inflammatory response and damage in the  
331 respiratory tract of mice.

### 332 **Bacterial load and inflammatory cytokines in the blood of mice infected by *T.*** 333 ***pyogenes***

334 The dynamic of bacterial load in the peripheral blood of infected mice was also  
335 investigated. In agreement with our previous report (17), no bacteria were detected in  
336 the blood during the first two days of infection, while bacteria were detectable at 4 dpi  
337 (66.67 CFU/mL) and increased substantially by 7 dpi (366.67 CFU/mL) (Fig. 5A).  
338 However, bacterial loads in the lungs could be detected at 1 dpi and 2 dpi ( $1.44 \times 10^5$   
339 CFU/g and  $1.58 \times 10^5$  CFU/g, respectively), and bacteria levels increased strikingly at

340 4 dpi and 7 dpi ( $4.78 \times 10^5$  CFU/g and  $2.39 \times 10^6$  CFU/g, respectively).

341 It is well known that airway contraction and inflammatory responses are regulated by  
342 multiple cytokines (23). To investigate the effect of *T. pyogenes* on cytokine  
343 production in mice, typical pro- and anti-inflammatory cytokines in serum were  
344 examined by ELISA kits. After *T. pyogenes* infection, IL-1 $\beta$  increased significantly at  
345 1 dpi, and decreased at 2, 4 and 7 dpi compared to 1 dpi (Fig. 5B). IL-6 was increased  
346 significantly at 1 dpi (24.89 pg/mL) and peaked at 2 dpi (34.50 pg/mL) (Fig. 5C).  
347 TNF- $\alpha$  and IFN- $\gamma$  were both significantly increased at all time-points (Fig. 5D and E),  
348 peaking at 4 dpi (247.34 pg/mL) and 1 dpi (865.29 pg/mL), respectively. IL-10  
349 significantly increased ( $P < .001$ ) at 4 dpi and 7 dpi (Fig. 5F).

# 350 ***T. pyogenes* activates inflammasome, MAPK, Akt and NF- $\kappa$ B signaling pathways** 351 **in the lung of infected mice**

352 To identify whether the inflammasome is activated in response to *T. pyogenes*  
353 infection, we used four different antibodies to detect inflammasome complexes in  
354 lung tissue by western blot (Fig. 6). The results showed that NLRP1 and NLRC4  
355 expression (Figs. 6A and B) increased significantly between 2 and 7 dpi, while  
356 NLRP3 increased significantly only at 7 dpi (Fig. 6C) and AIM-2 was not expressed  
357 (data not shown). *T. pyogenes* clearly induced ASC expression and cleavage of  
358 pro-caspase-1, with both significantly increased from 1 dpi to 7 dpi ( $P < .001$ ) (Fig.  
359 6D and E). Moreover, GSDMD expression decreased significantly between 2 and 7  
360 dpi (Fig. 6F), whereas GSDMD-N and GSDMD-C were significantly increased from  
361 1 dpi to 7 dpi (Fig. 6G and H), suggesting pyroptosis occurred and released numerous

362 pro-inflammatory cytokines into the infected lungs. Indeed, western blot showed a  
363 marked increase in IL-1 $\beta$  and IL-18 (Fig. 6I and J) during infection, MMP9 increased  
364 significantly at 1 dpi (Fig. 6K), whereas MIF had no significant changes (Fig. 6L).  
365 In order to explore the mechanism of how *T. pyogenes* may induce inflammation, we  
366 also studied the effect of infection on the MAPK signaling pathways. Western blot  
367 was used to detected classical inflammation-related signaling kinases including JNK,  
368 ERK and p38 of the MAPK pathway in lungs of infected mice. The levels of p-JNK  
369 and p-ERK were increased and the ratio of p-JNK/JNK was increased significantly  
370 from 2 dpi to 7 dpi (Fig. 7A), while the ratio of p-ERK/ERK and p-p38/p38 also  
371 increased significantly from 1 dpi to 7 dpi (Fig. 7B and C). Moreover, we tested the  
372 activation status of the canonical Akt and NF- $\kappa$ B pathways, which are reported to be  
373 involved in movement of immunocytes from the peripheral blood to sites of  
374 inflammation. The ratio of p-AKT/AKT was significantly increased throughout the  
375 study ( $P < .001$ ) (Fig. 7D) and phosphorylation of NF- $\kappa$ B (Fig. 7E) was increased at 1,  
376 4 and 7 dpi.

### 377 **Caspase-independent and -dependent apoptosis pathways involved in lungs of** 378 **mice by *T. pyogenes* infection**

379 To determine whether *T. pyogenes* induced apoptosis in the lungs of infected mice,  
380 confocal microscopy was used to detect staining by TUNEL assay. Apoptotic signals  
381 were found not only in bronchial epithelial cells but also in the alveoli (Fig. 8A and B),  
382 which suggested *T. pyogenes* could induce apoptosis in the lungs of infected mice.  
383 Next, we used western blot to determine which type of signaling was induced by *T.*

384 *pyogenes* infection. As shown in Fig. 8C, the expression of AIF protein increased  
385 significantly at 1 and 2 dpi compared with the control group. In addition, there was a  
386 significant increase in caspase-3 (Casp3) and caspase-8 (Casp8) throughout the study  
387 (Fig. 8D and E). Meanwhile, cleaved caspase-3 (c-Casp3) also increased significantly  
388 except 2 dpi and cleaved caspase-8 (c-Casp8) increased from 1 dpi to 4 dpi (Fig. 8F  
389 and G), whereas caspase-9 no significant change (Fig. 8H). These results suggest the  
390 involvement of an AIF-mediated apoptosis pathway and a caspase-dependent pathway  
391 in *T. pyogenes*-induced apoptosis.

### 392 **TNF- $\alpha$ plays a role in apoptosis and inflammatory injury in the bronchiolar** 393 **epithelium**

394 The level of caspase-8 significantly increased throughout at least the first 7 days of *T.*  
395 *pyogenes* infection, suggesting that the TNF signaling pathway may be activated.  
396 Thus, we infected TNF- $\alpha^{-/-}$  mice to verify the role of TNF- $\alpha$  in apoptosis and lung  
397 damage. Apoptosis was detected using a TUNEL assay, and cell nuclei were stained  
398 with DAPI. As shown in Fig. 9A, there was less apoptotic signals were found in  
399 bronchial epithelial cells of TNF- $\alpha^{-/-}$  mice at 2 dpi, and the number of apoptotic cells  
400 in the infected TNF- $\alpha^{-/-}$  mice decreased significantly compared with the WT group  
401 (Fig. 9B). Furthermore, western blot analysis confirmed that the expression of  
402 caspase-8, caspase-3 and AIF decreased significantly compared with the WT group,  
403 while caspase-9 did not change significantly (Fig. 9C). Moreover, pathological  
404 sections of lung and trachea of TNF- $\alpha^{-/-}$  mice were observed. As shown in Fig. 9D, in  
405 the WT group, a large number of inflammatory cells infiltrated in parenchyma of lung



on 2 dpi. Trachea mucosal epithelial cells partially denatured, inflammatory cells infiltrated the submucosa, and the arrangement of bronchiolar/tracheal epithelial cells was more disordered compared with TNF- $\alpha^{-/-}$  group on 2 dpi. Whereas, in the infected TNF- $\alpha^{-/-}$  mice, less inflammatory cell infiltration in parenchyma of lung compared with WT group. Trachea mucosal epithelial cells showed slight degeneration and the arrangement of epithelial cells was more ordered than that seen with infection of WT mice on 2 dpi. Altogether, these data suggest that TNF- $\alpha$  plays a role in apoptosis and inflammatory injury to the bronchiolar epithelium of *T. pyogenes*-infected mice.

## Discussion

Currently, there have less studies on the effect of *T. pyogenes* on lung functions *in vitro*. Well differentiated PBECs and PCLS make it possible to analyze the host-pathogen interaction *in vitro*, including the initial events of immune activation (24). Here we show that *T. pyogenes* is able to interact with PBECs and PCLS, where induce immune responses and develop airway damage.

In this study, notable bronchoconstriction was observed and IL-4 increase in the supernatants of infected PCLS. Since IL-4 is associated with the pathogenesis of allergic disorders in humans (25), we speculate that its increase may contribute to the bronchoconstriction, especially in the high-dose group. The mechanisms underlying IL-4 mediation of porcine bronchial constriction need to be further investigated. *T. pyogenes* could adhere to ciliated respiratory epithelial cells, growing either on surface of bronchus or within bronchoconstricted areas. Bronchoconstriction can reduce the elimination capability of ciliated cells (26). Thus, *T. pyogenes*-induced

bronchoconstriction may help their proliferation within constricted areas. Furthermore, *T. pyogenes* destroyed the integrity of airway epithelium under ALI conditions, which may facilitate their movement across physical barrier of respiratory epithelium. It has been reported that the sulysin of *Streptococcus suis* can induce apoptosis of epithelial cells under ALI conditions (10). The genotype of 20121 is *plo*<sup>+</sup>/*fimA*<sup>+</sup>/*fimE*<sup>+</sup>/*nanH*<sup>+</sup>/*nanP*<sup>+</sup> (17). Thus, hemolysin (pyolysin, *plo*) may accumulate locally in *T. pyogenes*-colonized areas under ALI conditions, inducing damage to epithelial cells. This will be further verified in future studies.

The release of LDH is used to measure cytotoxicity, LDH also can be released by cells undergoing pyroptosis [36]. In this study, *T. pyogenes* induce the cytotoxicity in well-differentiated PBECs (Fig. 1A) and PCLS (Fig. 2C). According to Fig. 1A, the discontinuous cytotoxic effect may be dependent on the number of bacteria. Non-adherent bacteria were removed at 4 hpi, and those attached were too few to induce detectable cytotoxic effect at 24 hpi. Subsequently, *T. pyogenes* proliferated, reaching a threshold to manifest cytotoxicity at 48 hpi. We also test the levels of IL-1 $\beta$  and IL-18 in PCLS, which are released from pyrolyzed cells. Both IL-1 $\beta$  and IL-18 increase from 4 hpi to 72 hpi. Accordingly, the LDH increase from 4 hpi to 72 hpi, which may be contributed by pyroptosis.

*T. pyogenes* usually produces a purulent-necrotic inflammation in the lung of clinically diseased swine (5), a process regulated by cytokines. Our results confirmed that *T. pyogenes* could induce the secretions of pro-inflammatory cytokines and anti-inflammatory cytokines in PCLS and mice, which is related to the polarization of

Th1 and Th2. In infected mice, pro-inflammatory serum cytokines as interleukin (IL)-1 $\beta$ , IL-6, TNF- $\alpha$ , IFN- $\gamma$  are produced, which suggested type 1 T-helpers (Th1) are involved in the reaction to antigen. IL-10, a typical anti-inflammatory cytokine, was secreted in serum of *T. pyogenes* infected mice significantly increased at 4 and 7 dpi rather than at 1 and 2 dpi, which may be related to high level Th1-proinflammatory cytokine IFN- $\gamma$  that inhibited Th2-polarized responses and suppress IL-10 synthesis. Our results suggested *T. pyogenes* induced a strong pro-inflammatory response at the early stage of mice infection, but anti-inflammatory process appeared relatively late. However, IL-10 significantly increased only in the  $8 \times 10^5$  CFU-infected PCLS group at 4 hpi rather than at 24 or 72 hpi. The time of the emergence of IL-10 is different *in vitro* and *in vivo*. The specific mechanism remains to be further studied.

In this study, *T. pyogenes* infection of PCLS and mice activated the inflammasome, which activated caspase-1, which then promoted cleavage of pro-inflammatory mediators IL-1 $\beta$  and IL-18 into their mature states (Fig.3). IL-1 $\beta$  and IL-18 are the most potent and first to be produced, which bind to their receptors to recruit and activate other inflammatory cells. IL-1 $\beta$  and IL-18 increased significantly after *T. pyogenes* infection of PCLS and mice, along with MMP9 and MIF. At the site of inflammation, MMP9 is often found synchronous with IL-1 $\beta$  (30), and MIF is considered to have a strong pro-inflammatory effect (31). This is the first report that *T. pyogenes* can induce secretion of pro-inflammatory cytokines in PCLS. Meanwhile, activation of the NF- $\kappa$ B pathway, which promotes the expression of pro-inflammatory cytokines including IL-6 and TNF- $\alpha$  in PCLS and mice (Fig.10). The

472 NLR-ASC-caspase-1 axis and NF- $\kappa$ B pathway were involved in both PCLS and mice,  
473 which confirm PCLS provide a platform to analyze the early pulmonary immune  
474 response. In addition, the increased phosphorylation of JNK, ERK and AKT in mice  
475 suggested the MAPK and Akt pathways also were involved in the observed  
476 inflammation (Fig. 10).

477 Since TNF- $\alpha$  and caspase-8 significantly upregulated in infected mice, which  
478 indicated that the TNF signaling pathway may be activated. To better understand the  
479 mechanism of leading to degeneration of epithelial cells of lungs in infected mice, we  
480 used *T. pyogenes* to infect TNF- $\alpha^{-/-}$  mice, found *T. pyogenes*-induced apoptosis and  
481 degeneration of epithelial cells in lungs of TNF- $\alpha^{-/-}$  mice were alleviated. So  
482 pro-inflammatory TNF- $\alpha$  plays an important role in apoptosis and lung injury induced  
483 by *T. pyogenes*. Collectively, *T. pyogenes* infection caused significant inflammatory  
484 responses in respiratory system, a variety of pro-inflammatory cytokines were  
485 produced, which are unrestricted by regulatory mediators, resulting in degeneration of  
486 epithelial cells (Fig. 10). Therefore, blocking NLR inflammasome activation to  
487 prevent large amounts of pro-inflammatory cytokines production early in infection, as  
488 well as treatments targeting TNF, may slow the disease progression in the early of  
489 infection.

490 In conclusion, we investigated the role of inflammation in *T. pyogenes*-induced  
491 bronchiolar epithelium damage *in vitro* and *in vivo*. NLR/ASC/caspase-1/IL axis and  
492 NF- $\kappa$ B pathway play the greatest role in inflammation and contribute to bronchiolar  
493 epithelium damage during *T. pyogenes* infection.

494

## 495 **Conclusion**

496 The role of inflammation in *T. pyogenes*-induced bronchiolar epithelium damage are  
497 investigated *in vitro* and *in vivo*, highlighting the mechanism underlying pathological  
498 development in respiratory system during *T. pyogenes* infection.

499

## 500 **Author contributions**

501 SW, FM and XC conceived the study and designed the experimental procedures. LQ,  
502 FM and SL performed the experiments. LQ, FM, HH, WZ and SW analysed the data.  
503 HH, HZ, YS, WZ, TA and XC contributed reagents and materials. LQ, FM and SW  
504 wrote the manuscript.

505

## 506 **Acknowledgements**

507 This work was supported by the National Natural Science Foundation of China  
508 (32273018), the Central Public-interest Scientific Institution Basal Research Fund  
509 (NO.1610302022006) and Heilongjiang pig Modern Agricultural Technology  
510 Collaborative Innovation System.

511

## 512 **Competing interest**

513 None declared.

514

## 515 **References**

- 516 1. Qi M, Liu J, Jiang Q, Niu H, Wang X, Zhou D, Lin P, Chen H, Wang A, Jin Y. 2021. *Trueperella*  
517 *pyogenes* pyolysin inhibits lipopolysaccharide-induced inflammatory response in  
518 endometrium stromal cells via autophagy- and ATF6-dependent mechanism. *Braz J Microbiol*  
519 52:939-952.
- 520 2. Ahmed MFE, Alssahen M, Lammler C, Eisenberg T, Plotz M, Abdulmawjood A. 2020. Studies  
521 on *Trueperella pyogenes* isolated from an okapi (*Okapia johnstoni*) and a royal python  
522 (*Python regius*). *BMC Vet Res* 16:292.
- 523 3. Dong WL, Kong LC, Wang Y, Gou CL, Xu B, Ma HX, Gao YH. 2017. Aminoglycoside resistance of  
524 *Trueperella pyogenes* isolated from pigs in China. *J Vet Med Sci* 79:1836-1839.
- 525 4. Rzewuska M, Czapowicz M, Gawryś M, Markowska-Daniel I, Bielecki W. 2016. Relationships  
526 between antimicrobial resistance, distribution of virulence factor genes and the origin of  
527 *Trueperella pyogenes* isolated from domestic animals and European bison (*Bison bonasus*).  
528 *Microb Pathog* 96:35-41.
- 529 5. Jarosz Ł S, Gradzki Z, Kalinowski M. 2014. *Trueperella pyogenes* infections in swine: clinical  
530 course and pathology. *Pol J Vet Sci* 17:395-404.
- 531 6. Ribeiro MG, Riseti RM, Bolaños CA, Caffaro KA, de Moraes AC, Lara GH, Zamprogna TO, Paes  
532 AC, Listoni FJ, Franco MM. 2015. *Trueperella pyogenes* multispecies infections in domestic  
533 animals: a retrospective study of 144 cases (2002 to 2012). *Vet Q* 35:82-7.
- 534 7. Ganesan S, Comstock AT, Sajjan US. 2013. Barrier function of airway tract epithelium. *Tissue*  
535 *Barriers* 1:e24997.
- 536 8. Lam E, Ramke M, Groos S, Warnecke G, Heim A. 2011. A differentiated porcine bronchial  
537 epithelial cell culture model for studying human adenovirus tropism and virulence. *J Virol*  
538 *Methods* 178:117-23.
- 539 9. Wu NH, Yang W, Beineke A, Dijkman R, Matrosovich M, Baumgärtner W, Thiel V,  
540 Valentin-Weigand P, Meng F, Herrler G. 2016. The differentiated airway epithelium infected  
541 by influenza viruses maintains the barrier function despite a dramatic loss of ciliated cells. *Sci*  
542 *Rep* 6:39668.
- 543 10. Meng F, Wu NH, Seitz M, Herrler G, Valentin-Weigand P. 2016. Efficient suilysin-mediated  
544 invasion and apoptosis in porcine respiratory epithelial cells after streptococcal infection  
545 under air-liquid interface conditions. *Sci Rep* 6:26748.
- 546 11. Meng F, Tong J, Vötsch D, Peng JY, Cai X, Willenborg M, Herrler G, Wu NH, Valentin-Weigand P.  
547 2019. Viral Coinfection Replaces Effects of Suilysin on *Streptococcus suis* Adherence to and  
548 Invasion of Respiratory Epithelial Cells Grown under Air-Liquid Interface Conditions. *Infect*  
549 *Immun* 87.
- 550 12. Meng F, Punyadarsaniya D, Uhlenbruck S, Hennig-Pauka I, Schwegmann-Wessels C, Ren X,  
551 Dürrwald R, Herrler G. 2013. Replication characteristics of swine influenza viruses in  
552 precision-cut lung slices reflect the virulence properties of the viruses. *Vet Res* 44:110.
- 553 13. Fiole D, Deman P, Trescos Y, Mayol JF, Mathieu J, Vial JC, Douady J, Tournier JN. 2014.  
554 Two-photon intravital imaging of lungs during anthrax infection reveals long-lasting  
555 macrophage-dendritic cell contacts. *Infect Immun* 82:864-72.
- 556 14. Ågren L, Elfsmark L, Akfur C, Jonasson S. 2021. High concentrations of ammonia induced  
557 cytotoxicity and bronchoconstriction in a precision-cut lung slices rat model. *Toxicol Lett*  
558 349:51-60.
- 559 15. Delgado-Ortega M, Melo S, Punyadarsaniya D, Ramé C, Olivier M, Soubieux D, Marc D, Simon

560 G, Herrler G, Berri M, Dupont J, Meurens F. 2014. Innate immune response to a H3N2  
561 subtype swine influenza virus in newborn porcine trachea cells, alveolar macrophages, and  
562 precision-cut lung slices. *Vet Res* 45:42.

563 16. Wu W, Zhang W, Booth JL, Metcalf JP. 2012. Influenza A(H1N1)pdm09 virus suppresses RIG-I  
564 initiated innate antiviral responses in the human lung. *PLoS One* 7:e49856.

565 17. Qin L, Meng F, He H, Yang YB, Wang G, Tang YD, Sun M, Zhang W, Cai X, Wang S. 2021. A  
566 Virulent *Trueperella pyogenes* Isolate, Which Causes Severe Bronchoconstriction in Porcine  
567 Precision-Cut Lung Slices. *Front Vet Sci* 8:824349.

568 18. Farsani SM, Deijs M, Dijkman R, Molenkamp R, Jeeninga RE, Ieven M, Goossens H, van der  
569 Hoek L. 2015. Culturing of respiratory viruses in well-differentiated pseudostratified human  
570 airway epithelium as a tool to detect unknown viruses. *Influenza Other Respir Viruses* 9:51-7.

571 19. Meng F, Wu NH, Nerlich A, Herrler G, Valentin-Weigand P, Seitz M. 2015. Dynamic  
572 Virus-Bacterium Interactions in a Porcine Precision-Cut Lung Slice Coinfection Model: Swine  
573 Influenza Virus Paves the Way for *Streptococcus suis* Infection in a Two-Step Process. *Infect*  
574 *Immun* 83:2806-15.

575 20. Su A, Tong J, Fu Y, Muller S, Weldearegay YB, Becher P, Valentin-Weigand P, Meens J, Herrler G.  
576 2020. Infection of bovine well-differentiated airway epithelial cells by *Pasteurella multocida*:  
577 actions and counteractions in the bacteria-host interactions. *Vet Res* 51:140.

578 21. Jost BH, Trinh HT, Songer JG, Billington SJ. 2003. Immunization with genetic toxoids of the  
579 *Arcanobacterium pyogenes* cholesterol-dependent cytolysin, pyolysin, protects mice against  
580 infection. *Infect Immun* 71:2966-9.

581 22. Li J, Hu L, Liu Y, Huang L, Mu Y, Cai X, Weng C. 2015. DDX19A Senses Viral RNA and Mediates  
582 NLRP3-Dependent Inflammasome Activation. *J Immunol* 195:5732-49.

583 23. Remot A, Descamps D, Noordine ML, Boukadiri A, Mathieu E, Robert V, Riffault S, Lambrecht  
584 B, Langella P, Hammad H, Thomas M. 2017. Bacteria isolated from lung modulate asthma  
585 susceptibility in mice. *ISME J* 11:1061-1074.

586 24. Bryson KJ, Garrido D, Esposito M, McLachlan G, Digard P, Schouler C, Guabiraba R, Trapp S,  
587 Vervelde L. 2020. Precision cut lung slices: a novel versatile tool to examine host-pathogen  
588 interaction in the chicken lung. *Vet Res* 51:2.

589 25. Oh CK, Geba GP, Molfino N. 2010. Investigational therapeutics targeting the IL-4/IL-13/STAT-6  
590 pathway for the treatment of asthma. *Eur Respir Rev* 19:46-54.

591 26. Huffnagle GB, Dickson RP. 2015. The bacterial microbiota in inflammatory lung diseases. *Clin*  
592 *Immunol* 159:177-82.

593 27. Gądek-Michalska A, Bugajski J. 2010. Interleukin-1 (IL-1) in stress-induced activation of  
594 limbic-hypothalamic-pituitary adrenal axis. *Pharmacological Reports* : PR 62:969-982.

595 28. Koo JW, Duman RS. 2008. IL-1 $\beta$  is an essential mediator of the antineurogenic and  
596 anhedonic effects of stress. *Proceedings of the National Academy of Sciences of the United*  
597 *States of America* 105:751-756.

598 29. Zefferino R, Di Gioia S, Conese M. 2021. Molecular links between endocrine, nervous and  
599 immune system during chronic stress. *Brain and Behavior* 11:e01960.

600 30. Dai J, Shen J, Chai Y, Chen H. 2021. IL-1 $\beta$  Impaired Diabetic Wound Healing by Regulating  
601 MMP-2 and MMP-9 through the p38 Pathway. *Mediators Inflamm* 2021:6645766.

602 31. Harris J, VanPatten S, Deen NS, Al-Abed Y, Morand EF. 2019. Rediscovering MIF: New Tricks for  
603 an Old Cytokine. *Trends Immunol* 40:447-462.

604

605



606

# Figure Legends

607 **Figure 1. Cytotoxicity and *T. pyogenes*-induced damage to well-differentiated**

608 **porcine bronchial epithelial cells.** PBECs were apically infected with approximately

609  $8 \times 10^5$  CFU of *T. pyogenes* and washed thoroughly to remove non-adherent bacteria

610 after 4 h and further incubated under ALI conditions. **(A)** Cytotoxic effects of *T.*

611 *pyogenes* on porcine bronchial epithelial cells (PBECs) grown under air-liquid

612 interface (ALI) conditions were quantified by a standard LDH-release assay. Results

613 are expressed as % cytotoxicity compared to 100% killed cells condition and

614 expressed as mean  $\pm$  SD; \*\*\*,  $P < .001$ , determined using one-way ANOVA and

615 Tukey's multiple comparison test. Experiments were performed three times. **(B)**

616 Immunostaining was performed to visualize cilia (red) and *T. pyogenes* (green), and

617 nuclei were stained by DAPI (blue). Bars represent 20  $\mu$ m in horizontal sections for

618 upper images, and lower images are the orthogonal views of Z-stacks (white dotted

619 line) as shown in YZ section at 4 hpi and 72 hpi or XZ section in Control (Ctr) and 24

620 hpi.

621 **Figure 2. Interaction between *T. pyogenes* with porcine precision-cut lung slices.**

622 Precision-cut lung slices (PCLS) were infected with  $8 \times 10^4$  or  $8 \times 10^5$  CFU/well of *T.*

623 *pyogenes* for 4 h and washed thoroughly to remove non-adherent bacteria. Cells were

624 fixed for cryosections at 4, 24 and 72 hpi and used for immunofluorescence staining.

625 **(A)** *T. pyogenes* is shown in green, cilia ( $\beta$ -tubulin) in red, and nuclei (DAPI) in blue.

626 **(B)** Bacterial burden of *T. pyogenes* on PCLS at 4, 24, 72 hpi. **(C)** *T.*

627 *pyogenes*-induced cytotoxicity on PCLS, expressed as % cytotoxicity compared to

100% killed cells condition. **(D)** IL-4 and **(E)** IL-10 levels in PCLS supernatant after incubation with *T. pyogenes*. **(F)** ELISA was used to determine the level of chemokine CXCL8 in culture supernatant. **(G)** Western blot analysis was used to determine the amount of IL-4 in the infected PCLS tissue at 4, 24 and 72hpi. The PCLS from 3 pigs and experiments were performed three times; \*:  $P < .05$ , \*\*:  $P < .01$ , \*\*\*:  $P < .001$ .

**Figure 3. The NLRP3 and NF- $\kappa$ B pathways are activated by *T. pyogenes* in PCLS.**

Precision-cut lung slices (PCLS) were challenged with  $8 \times 10^5$  CFU/well of *T. pyogenes* 20121 as described in the Experimental Procedure. Western blot analysis was used to detect of the levles of NLRP3 **(A)**, ASC **(B)**, Casp1(20) **(C)**, IL-1 $\beta$  **(D)**, IL-18 **(E)**, MMP9 **(F)**, MIF **(G)** and NF- $\kappa$ B **(H)** proteins; The relative protein expression levels were detected by Image J software and expressed as mean  $\pm$  SD; \*:  $P < .05$ , \*\*:  $P < .01$ , \*\*\*:  $P < .001$ .

**Figure 4. Histopathology lesions induced in the lungs of mice infected with *T.***

***pyogenes*.** Mice were infected with  $2 \times 10^6$  CFU of *T. pyogenes* strain 20121 and sacrificed at 1, 2, 4 and 7 dpi. Samples of **(A)** lung and **(B)** tracheas were fixed, embedded in paraffin and sectioned at a thickness of 5  $\mu$ m. Sections were stained with hematoxylin-eosin (HE), photographed using Zeiss Viewer software; the red box shows greater detail, with extensive inflammatory cell infiltration of the lung (red arrow) and epithelial cell degeneration (green box).

**Figure 5. Bacterial load and cytokine levels in the lungs and blood of *T. pyogenes***

**-infected mice. (A)** Bacterial load in lung (CFU/g of tissue) and blood (CFU/mL).

ELISA was used to detect the levels of **(B)** IL-1 $\beta$ , **(C)** IL-6, **(D)** TNF- $\alpha$  **(E)** IFN- $\gamma$

650 and (F) IL-10 in serum samples. Data are shown as the mean  $\pm$  SD of the  
651 independent experiments; \*:  $P < .05$ , \*\*:  $P < .01$ , \*\*\*:  $P < .001$ .

652 **Figure 6. The NLR/ASC/caspase-1/IL axis is activated in the lungs of *T.***  
653 ***pyogenes*-infected mice.** Western blots of *T. pyogenes*-infected wild type mice lungs  
654 at 1, 2, 4 and 7 dpi are shown. Relative protein expression of (A) NLRP1, (B) NLRC4,  
655 (C) NLRP3, (D) ASC, (E) Casp1(p20), (F) GSDMD, (G) GSDMD-N, (H)  
656 GSDMD-C, (I) IL-1 $\beta$ , (J) IL-18, (K) MMP9 and (L) MIF are shown; \*:  $P < .05$ , \*\*:  $P < .01$ , \*\*\*:  $P < .001$ .

658 **Figure 7. Comparison of protein expression of molecules related to activation of**  
659 **the MAPK pathway and inflammatory response in the lungs of mice after**  
660 **challenge with *T. pyogenes*.** Representative western blots shows the expression and  
661 phosphorylation level of (A) JNK, (B) ERK, (C) p38, (D) AKT and (E) NF- $\kappa$ B. The  
662 mean  $\pm$  SD of three experiments are shown; \*:  $P < .05$ , \*\*:  $P < .01$ , \*\*\*:  $P < .001$ .

663 **Figure 8. *T. pyogenes* infection induces apoptosis in mice lung cells.** (A) Mice were  
664 challenged with  $2 \times 10^6$  CFU of *T. pyogenes*, and at 2 dpi, lungs were collected for  
665 immunofluorescence to verify the occurrence of apoptosis using a TUNEL assay.  
666 Apoptosis is shown red in (A) bronchial epithelial cells and (B) pulmonary alveoli in  
667 lung, and nuclei (DAPI) in blue, and the white box indicates the part view of the  
668 higher magnification images. Western blot analysis of (C) AIF, (D) caspase-3 (Casp3),  
669 (E) caspase-8 (Casp8), (F) cleaved caspase-3 (c-Casp3), (G) cleaved caspase-8  
670 (c-Casp8), (H) caspase-9 (Casp9) expression shows apoptosis of lung cells at different  
671 days of infection. Data are shown as the mean  $\pm$  SD of three experiments. \*:  $P < .05$ ,

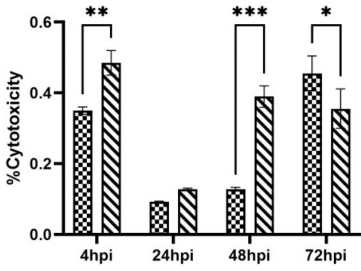
672 \*\*:  $P < .01$ , \*\*\* $P < .001$ .

673 **Figure 9. Apoptosis and injury induced by *T. pyogenes* alleviated in Lungs of**  
 674 **TNF- $\alpha^{-/-}$  mice.** Wild type (WT) and TNF- $\alpha^{-/-}$  C57 (KO) mice were challenged with  
 675  $2 \times 10^6$  CFU of *T. pyogenes*, and at 2 dpi, lungs were collected for immunofluorescence.  
 676 (A) Apoptotic cells (TUNEL) in trachea epithelial cells were detected with the In Situ  
 677 Cell Death Detection Kit, and cell nuclei were stained with DAPI. (B) Number of  
 678 apoptotic cells in trachea epithelial cells from different groups of mice. \*\*\* $p < .001$ .  
 679 Protein levels of (C) caspase-8, caspase-9, caspase-3 and AIF were detected by  
 680 western blot. (D) Comparison of histopathological lesions of lungs and tracheas  
 681 between infected WT and KO mice on 2 dpi, showing the epithelial layer of the  
 682 respiratory tract of lungs (red dotted boxes) and neutrophil (red arrow).

683 **Figure 10. A schematic overview summarizing the main mechanism of epithelial**  
 684 **cell injury.** *T. pyogenes* infection triggers NF- $\kappa$ B to enter the nucleus, where it  
 685 promotes expression of pro-inflammatory factors and the NLR inflammasomes.  
 686 Meanwhile, *T. pyogenes* can directly promote the assembly and formation of the NLR  
 687 inflammasome. Pyroptosis happens via NLR-ASC-caspase-1-GSDMD pathway,  
 688 which promotes the release of mature IL-18, IL-1 $\beta$  and other pro-inflammatory  
 689 factors into the extracellular, then cause inflammatory lung tissue injury. For example,  
 690 TNF- $\alpha$  increases and induces epithelial cells apoptosis via TNF receptor pathway.

691

**A**



**B**

